1 # Global source apportionment of aerosols into major emission regions

2 # and sectors over 1850–2017

5 Yang Yang[1*], Shaoxuan Mou[1], Hailong Wang[2], Pinya Wang[1], Baojie Li[1], Hong Liao[1]

9 [1]Joint International Research Laboratory of Climate and Environment Change (ILCEC),

10 Jiangsu Key Laboratory of Atmospheric Environment Monitoring and Pollution Control,

11 Jiangsu Collaborative Innovation Center of Atmospheric Environment and Equipment

12 Technology, School of Environmental Science and Engineering, Nanjing University of

13 Information Science and Technology, Nanjing, Jiangsu, China

14 [2]Atmospheric, Climate, and Earth Sciences Division, Pacific Northwest National Laboratory,

15 Richland, Washington, USA

21 *Correspondence to yang.yang@nuist.edu.cn

Abstract

Anthropogenic emissions of aerosols and precursor gases have been changing significantly in the past few decades across the world. In this study, an explicit aerosol source tagging system (EAST) is merged into the Energy Exascale Earth System Model version 1 (E3SMv1) to quantify the variations in anthropogenic aerosol concentrations, source contributions, and their subsequent radiative impact in four major emission regions on the globe during 1850–1980, 1980–2010 and 2010–2017. In North America and Europe, changes in anthropogenic $PM_{2.5}$ were mainly caused by changes in emissions from local energy and industrial sectors. The local industrial sector caused the most increase in $PM_{2.5}$ in East Asia during1980–2010 and decrease during 2010–2017. In South Asia, the increase in energy-related emissions dominated the rise of $PM_{2.5}$ levels during 1980–2017. During 1850–1980, the increases in emissions from North America contributed to the increase in European $PM_{2.5}$ burden by 1.7 mg m^{-2} and the sources from the Europe were also responsible for the $PM_{2.5}$ burden increase in East Asia and South Asia by about 1.0 mg m^{-2}. During 1980–2010, East Asia contributed to an increase of 0.4–0.6 mg m^{-2} in $PM_{2.5}$ burden in North America and Europe, while South Asian contributed about 0.3 mg m^{-2}. During 2010–2017, the contributions from East Asia to the $PM_{2.5}$ burdens in the North America, Europe and South Asia declined by 0.3–0.6 mg m^{-2} due to Clean Air actions in China, while the contributions from South Asia still increased due to the continuous increase in emissions in South Asia. The historical changes in aerosols had an impact on effective radiative forcing through aerosol-radiation interactions (ERF_{ari}). During 1980–2010, a decline in North American aerosols resulted in a positive ERF_{ari} change (warming effect) in Europe and a decline of aerosols in Europe caused a warming effect in

44   Russia and northern China. The changes in ERF_{ari} from the increase and decrease of aerosols

45   in China during 1980–2010 and 2010–2017, respectively, are comparable in magnitude. The

46   continuous aerosol increases in South Asia from 1980 to 2017 resulted in negative ERF_{ari}

47   (cooling) changes in South Asia, Southeast Asia, and southern China.

1. Introduction

Atmospheric aerosols, also known as particulate matter (PM), have significant influences on air quality and human health (Anenberg et al., 2010; Finlayson-Pitts and Pitts, 1997; Li et al., 2017; Pöschl, 2005). Aerosols also affect the energy budget of the earth system by scattering and/or absorbing solar radiation, thus directly affecting the climate (Gao et al., 2022; Yang et al., 2020a, 2023; Wang et al., 2023). Meanwhile, they may act as cloud condensation nuclei and/or ice nuclei, changing cloud characteristics and atmospheric water cycle, which indirectly affect the climate (Liao et al., 2015; Lohmann and Feichter, 2005; Rosenfeld et al., 2008; Yang et al., 2022a). Due to the absorption of solar radiation, aerosol-induced heating can strengthen temperature inversion and increase the atmospheric stability, which inhibits the vertical mixing and transport of aerosols and leads to a further increase in near-surface aerosol concentrations (Chen et al., 2021; Lou et al., 2019). Therefore, knowing the sources of aerosols and their variations have become a vital direction in the field of environmental and atmospheric sciences.

Human activities have a great influence on global aerosol distributions and compositions. For example, many countries have taken various air quality control measures at different stages of their economic development, causing distinct historical temporal changes of aerosol emissions across the world. Since the start of industrialization, anthropogenic emissions of aerosols and precursor gases have substantially increased, which significantly affected the atmospheric environment and the Earth's energy balance (Carslaw et al., 2013). European and North American countries became major contributors of pollutant emissions. Since the 1980s, coal emissions have declined steadily in Europe and North America owing to the legislation

70 and effective environmental policies to reduce local anthropogenic emissions of aerosol and

71 precursor gases (Smith et al., 2011). In contrast to North America and Europe, the coal

72 consumption in China and India has experienced a substantial increase and anthropogenic

73 emissions from these regions continued to rise (Hoesly et al., 2018; Lim et al., 2020). Zheng et

74 al. (2018) also reported that due to active clean air policies and the emission control of power

75 plants and industry, anthropogenic emissions of $PM_{2.5}$ (particulate matter less than 2.5 μm in

76 diameter) from China have significantly decreased by 33% during 2013–2017. However,

77 countries in South Asia still rely on coal and petroleum and thus aerosol emissions from South

78 Asia have kept increasing in recent years (Li et al., 2017).

79   Regional aerosol pollution can be induced by both local emissions and long-range

80 transport of pollutants across regions, countries or even continents, which impose a far-

81 reaching impact on air quality and human health (Akimoto, 2003; Anenberg et al., 2014; Jaffe

82 et al., 1999; Lin et al., 2014; Liu et al., 2009; Zhang et al., 2017). Studies reported that the air

83 quality in Europe is largely impacted by the long-range aerosol transport from North America

84 (Stohl and Trickl, 1999; Yang et al., 2018a, 2020b). Asian anthropogenic emissions in spring

85 also have a significant effect on the aerosol concentrations in North American (Jaffe et al.,

86 1999). Moreover, studies found that air pollution from Africa and Europe moved eastward and

87 merged with Asian pollution, affecting air quality in western North America (Liu et al., 2005;

88 Chin et al., 2007). Yang et al. (2017) also found that remote sources contributed the most to

89 the regions with low emissions through long-range transport, which further impacted the local

90 climate. Therefore, relying on the domestic emission control alone may be insufficient to

91 prevent air pollution due to the long-distance transport of air pollutants (Liu et al., 2009). A

92   study revealed that approximately 12% of global premature deaths caused by $PM_{2.5}$ were

93   related to non-local air pollutants (Zhang et al., 2017). About 16% of premature deaths in India

94   caused by $PM_{2.5}$ were attributed to aerosol transport from external source regions (David et al.,

95   2019). Within each emission source region, aerosols also come from different emission sectors.

96   Many scientific control measures and policies are implemented based on the source attribution

97   of air pollutants from individual sectors. Hence, it is of great significance to quantify source

98   contributions of long-range transport of aerosols from major emission regions of the world as

99   well as aerosols from major emission sectors.

100   Anthropogenic emissions of aerosols and precursor gases have changed significantly in

101   different source regions over the past century. Few studies focus on the source attributions of

102   aerosols across the globe over such a long period of time. In this study, we focus on the changes

103   in aerosols and emission source region and sector contributions in major source regions (i.e.,

104   North America, Europe, East Asia, South Asia) during the three important periods of emission

105   changes since industrialization (1850–1980, 1980–2010 and 2010–2017) based on the

106   Energy Exascale Earth System Model version 1 (E3SMv1), equipped with an explicit aerosol

107   source tagging system (E3SMv1-EAST).

108   **2. Methods**

109   **2.1. Model description and experimental design**

110   To study variations in historical anthropogenic aerosols in the major source regions, the

111   E3SMv1 developed by US Department of Energy (DOE) (Golaz et al., 2019) is used in this

112   study. The E3SMv1 model is updated on the basis of Community Atmosphere Model version

113   5 (CAM5) in order to explore several key emerging issues in the field of environment and

114 climate, and is a branch of the widely-used Community Earth System Model (CESM) (Rasch

115 et al., 2019). E3SMv1 consists of atmosphere, land surface, ocean, sea ice, and river model

116 components. It features numerous upgrades to aerosol, turbulence, chemical, and cloud-related

117 processes, offering multiple spatial resolution options. The model can run simulations for

118 decades or more at higher resolution to help understand past, present, and future changes in

119 Earth's behavior, and to explore how the atmosphere interacts with other components of the

120 Earth system. Aerosol microphysics and interactions with stratiform clouds are treated with the

121 four-mode Modal Aerosols Module (MAM4) (Liu et al., 2016), which predicts the mass and

122 number concentrations of sulfate, black carbon (BC), primary organic matter (POM),

123 secondary organic aerosol (SOA), marine organic aerosol, mineral dust and sea salt (Wang et

124 al., 2020). EAMv1 applies the "Morrison and Gettelman version 2" (MG2) two-moment bulk

125 microphysics parameterization for stratiform clouds (Gettelman and Morrison, 2015). It allows

126 aerosol-cloud interactions in all stratiform and shallow convective clouds but neglects in deep

127 convective clouds (Rasch et al., 2019). Liquid cloud drop activation is based on Abdul-Razzak

128 and Ghan (2000) and a classical nucleation theory-based ice nucleation parameterization for

129 the heterogeneous ice formation in mixed-phase clouds follows Y. Wang et al. (2014).

130 Hygroscopicity are specified for soluble aerosols to calculate the particle size based on relative

131 humidity. The aerosols are assumed to mix internally in the same aerosol mode and externally

132 between modes when calculating the aerosol optical properties (Ghan and Zaveri, 2007). The

133 model has been applied to investigate the variations in anthropogenic and natural aerosols

134 related to the air-sea interactions (Yang et al., 2022b; Zeng et al., 2021). Compared to the

135 regional model, the E3SMv1 with an aerosol tagging tool introduced in this study is more

136 suitable for the simulation of transboundary and intercontinental transport of aerosols across

137 the globe. In this study, the model is configured at its standard horizontal spatial resolution of

138 approximately 1° with 72 vertical layers.

139   Global emissions of aerosols and precursor gases used in the simulations are obtained

140 from the CMIP6 (the Coupled Model Intercomparison Project Phase 6) datasets (Hoesly et al.,

141 2018; van Marle et al., 2017). However, the anthropogenic emissions in China are replaced

142 with MEIC (Multi-resolution Emission Inventory for China) inventory, which fully considers

143 the implementation of clean air actions over China since the 2010s (Gao et al., 2022, 2023; Li

144 et al., 2021; Zheng et al., 2018). Following previous studies (Ren et al., 2021; Yang et al.,

145 2018a), the near-surface concentrations of $PM_{2.5}$ here are estimated as the sum of sulfate, BC,

146 POM and SOA concentrations. Effective radiative forcing (ERF) refers to the change of the

147 net radiative flux at the top of the atmosphere (TOA) after the external forcing is applied. In

148 this study, ERF due to aerosol-radiation interactions (ERF_{ari}) for the individual tagged source

149 regions is derived as the difference in TOA net radiative fluxes from a pair of diagnostic

150 radiation calculations with and without the particular tagged aerosols from the source regions

151 for the all-sky condition following Ghan (2013).

152   This study focuses on the variations in source region and sector contributions in four major

153 emission regions of the world (North America, Europe, East Asia and South Asia) during the

154 three key historical periods of emission changes (1850–1980, 1980–2010 and 2010–2017).

155 Four simulations with monthly anthropogenic emissions of aerosols and precursors fixed at the

156 1850, 1980, 2010 and 2017 levels, respectively, are conducted. All simulations are performed

157 for one year following 6-month model spin-up. Greenhouse gas concentrations, solar insolation,

158   sea surface temperature and sea ice extent are prescribed at the 2000 levels. The meteorological

159   fields including 3-dimentional temperature, specific humidity, and winds are nudged toward

160   the MERRA-2 (Modern-Era Retrospective Analysis for Research and Applications, version 2)

161   reanalysis (Gelaro et al., 2017) in year 2017 at a 6-hourly relaxation timescale.

162   **2.2. Explicit aerosol source tagging system**

163   Source apportionment aims to quantify the contributions to aerosols from specific sources.

164   To examine the source-receptor relationships of aerosols, we implemented the Explicit Aerosol

165   Source Tagging (EAST) in E3SMv1, which play a critical role in attributing aerosol

166   concentrations to their respective emission sources. The EAST follows the BC source-tagging

167   technique introduced in H. Wang et al. (2014), sulfate source-tagging method used in Yang et

168   al. (2017) and other carbonaceous aerosol-tagging applied in Yang et al. (2018a), which was

169   previously implemented in the Community Atmosphere Model version 5 (CAM5-EAST). This

170   tagging system is different from the traditional emission sensitivity method that zero out or

171   perturb emissions from a given source region or sector in sensitivity simulations along with a

172   baseline simulation, which has to assume a linear response to emission perturbation and

173   requires many additional simulations for estimating the contributions from multiple sources

174   (Wang et al., 2014). EAST independently considers all aerosol physical, chemical, and

175   dynamical processes for each tagged sources through introducing additional aerosol-related

176   variables within one simulation and it does not rely on a linear response to emission

177   perturbations. These capabilities make it physically more accurate and time saving than the

178   sensitivity experiments. This tagging method has previously been adopted in regional models

179   and has now implemented in the global E3SMv1 model to better understand the

180   intercontinental transport from sources outside the regional domain.

181   In this study, totally 18 tags are set for each anthropogenic species of aerosols and

182   precursors. Each of the 4 major source regions, including North America (NAM), Europe

183   (EUR), East Asia (EAS) and South Asia (SAS), has 4 tags for the energy transformation and

184   extraction (ENE), industrial combustion and processes (IND), residential, commercial and

185   other (RCO) and the rest of anthropogenic emission sectors (RST). One tag is assigned to the

186   anthropogenic emissions from rest of the world (ROW) and the last tag is allocated for all the

187   natural/biogenic sources including open biomass burning, volcanic emissions and oceanic

188   emissions.

189   **2.3. Model evaluation**

190   In order to evaluate the performance of E3SMv1 in reproducing the aerosol concentrations,

191   Fig. 2 compares the simulated near-surface $PM_{2.5}$ concentrations with the observations from

192   the Interagency Monitoring of Protected Visual Environments (IMPROVE) over the U.S., the

193   European Monitoring and Evaluation Programme (EMEP) over Europe, the U.S. embassies

194   and consulates in India and the China National Environmental Monitoring Center (CNEMC)

195   over China in year 2017. The model successfully reproduces the spatial distribution of $PM_{2.5}$

196   concentrations, with relatively high concentrations in eastern China, India and low

197   concentrations in the U.S. and Europe. The spatial correlation coefficient (R) between the

198   E3SMv1 simulated $PM_{2.5}$ concentrations and observations is +0.80. The model well reproduces

199   the $PM_{2.5}$ concentrations in the U.S. with the normalized mean biases (NMB) of -11%.

200   However, it largely underestimates the $PM_{2.5}$ concentrations in China and Europe, which has

201 also been revealed in several studies (e.g., Gao et al., 2018; Gao et al., 2023; Navinya et al.,

202 2020; Zeng et al., 2021). This discrepancy is partly because E3SMv1 only considers limited

203 aerosol species (BC, POM, SOA and sulfate) without including nitrate and ammonium aerosols

204 in the aerosol module. On the other hand, the overestimated wet scavenging at the mid- and

205 high latitudes and underestimated gas-to-particle conversion can also lead to the low bias (Zeng

206 et al., 2021). The evaluation in 2010 also shows similar high correlation and biases (Fig. S3).

207   In order to evaluate the model performance in reproducing the historical changes in

208 aerosol concentrations during the important periods of emission changes, the variations in near-

209 surface $PM_{2.5}$ concentrations are compared with observations (Fig. S4) and MERRA-2

210 reanalysis (Fig. S5). The model well reproduces the decreases in $PM_{2.5}$ concentrations in the

211 eastern U.S. and Europe and the increases in East Asia and South Asia during 1980–2010, with

212 the spatial R of 0.78 between model results and MERRA-2 data. The model also well simulates

213 the aerosol decline in North America, Europe, and East Asia and a continuous increase in South

214 Asia during 2010–2017, with the R of 0.81 between model results and observational data.

215 **3. Results**

216 **3.1. Historical changes in aerosols over major source regions**

217   Figure 3 shows the variations in anthropogenic emissions of sulfur dioxide (SO_2) during

218 the three key periods of historical emission changes from the tagged source regions. Since

219 industrialization, anthropogenic SO_2 emissions had rising trends during 1850–1980, especially

220 in Europe and North America. Due to the implementation of clean air actions in western

221 countries, SO_2 emissions in North America and Europe declined considerably during 1980–

222 2010, while the emissions in East Asia and South Asia continued to increase. After 2010, China

223   issued several clean air policies, which led to significant decreases in anthropogenic SO_2

224   emissions in East Asia, while the SO_2 emissions in South Asia kept increasing during 2010–

225   2017. The changes in anthropogenic BC and organic carbon (OC) emissions are similar to those

226   of SO_2 (shown in Figure S1 and S2).

227   The changes in near-surface mass concentrations (Fig. 4) and column burdens (Fig. 5) of

228   anthropogenic $PM_{2.5}$ contributed by the tagged source regions during the focused three

229   historical time periods follow the corresponding changes in anthropogenic emissions. Column

230   burden refers to the concentration of aerosols contained in the air column above a unit area,

231   which can better reflect the aerosol transport within the air column and is more related to the

232   aerosol radiative effect. The near-surface concentration of aerosols represents the concentration

233   of aerosols in the air near the surface (from 1000 to 997 hPa for model layer), which is more

234   related to air quality and human health. Local anthropogenic emission changes drove the $PM_{2.5}$

235   to reach its peak in 1980 in North America and Europe and then to decrease. The maximum

236    $PM_{2.5}$ appeared in 2010 in East Asia and the anthropogenic $PM_{2.5}$ level continued growing in

237   South Asia during 1850–2017, consistent with previous studies (Dey et al.,2020; Guttikunda

238   et al., 2022; Singh et al.,2023).

239   To explore which aerosol species contributed the most to the changes in $PM_{2.5}$ during the

240   focused three historical time periods, Figs. 6 and 7 illustrate the relative contributions of

241   individual aerosols to the simulated changes in near-surface $PM_{2.5}$ mass concentrations and

242   column burdens, respectively, in four major emission regions. In general, the historical changes

243   in anthropogenic $PM_{2.5}$ were primarily driven by the changes in sulfate. In North America, the

244   contribution of sulfate to near-surface $PM_{2.5}$ concentration (column burden) rose from 7%

245   (11%) in 1850 to 67% (81%) in 1980, then dropped to 52% (67%) in 2017. In Europe, sulfate

246   contribution changed from 24% (34%) in 1850 to 71% (85%) in 1980, then decreased to 50%

247   (68%) in 2017. In East Asia, sulfate contribution changes from 2% (6%) in 1850 to 51% (71%)

248   in 1980, then decreased to 33% (56%) in 2017. It is interesting that the $PM_{2.5}$ levels in East

249   Asia increased during 1980–2010, but the sulfate contribution decreased in this time period. It

250   is because the carbonaceous aerosols increased remarkably, which reduced the fractional

251   contribution of sulfate. The sulfate contribution to $PM_{2.5}$ concentration (column burden)

252   increased throughout the period of 1850–2017, from 2% (5%) to 42% (62%) in South Asia.

253   Note that the carbonaceous aerosols, especially POM, dominated the $PM_{2.5}$ in all four targeted

254   regions in 1850, resulting from the high heating demand from the residential sector.

255   **3.2 Changes in contributions from major source regions and sectors**

256   Figure 8 shows the relative contributions from local and remote anthropogenic sources to

257   the near-surface concentrations and column burdens of $PM_{2.5}$ in the four targeted regions in

258   2010. Local sources dominated the near-surface anthropogenic $PM_{2.5}$ concentrations over the

259   high emission regions including eastern China, eastern U.S. and Indo-Gangetic Plain, with

260   local contributions being higher than 90%. In the regions with low emissions, such as the

261   Tibetan Plateau, the anthropogenic $PM_{2.5}$ concentrations were largely contributed by the long-

262   range transport of aerosols. The spatial distributions of burden contribution are similar to those

263   of corresponding contribution near the surface, but the long-range transport contributed more

264   to the column burden than to the near-surface contribution due to the more efficient pollutant

265   transport in the free troposphere than within the boundary layer. The long-range transport

266   contributes 30%–35% of $PM_{2.5}$ burden in East Asia and South Asia and 50–55% in North

267   America and Europe, much higher than the 10%–25% for the near-surface concentrations over

268   the four targeted regions.

269   Since both local and remote emissions can contribute to the anthropogenic $PM_{2.5}$, it is

270   valuable to know the historical changes in these contributions, especially by the local sources

271   from individual emission sectors and by remote sources from major emission regions. Figure

272   9 illustrates changes in the local source contributions from major emission sectors to the near-

273   surface concentrations and column burdens of $PM_{2.5}$ during 1850–2017. In North America and

274   Europe, the historical changes in anthropogenic $PM_{2.5}$ were largely induced by changes in

275   emissions from the local energy (ENE) sector, followed by the industry (IND) sector, which

276   increased before 1980 and decreased afterward. In East Asia, ENE, IND and residential (RCO)

277   sector emissions all had significant contributions to the increases in $PM_{2.5}$ concentration and

278   burden from1850 to1980. Then the contribution from local IND sector showed the largest

279   increases from 1980 to 2010 and decreases from 2010 to 2017. In South Asia, the

280   anthropogenic $PM_{2.5}$ increases from 1850 to 1980 were mainly attributed to the RCO emission

281   increases. After that, increases in ENE emissions dominated the rising $PM_{2.5}$ levels in South

282   Asia during 1980–2017.

283   Figure 10 presents changes in remote emission contributions from the tagged source

284   regions to the column burdens of $PM_{2.5}$ during 1850–2017. The contributions from long-range

285   transport to the near-surface concentrations and their historical variations over the four major

286   emissions regions are relatively small, which were also reported in previous studies (e.g., Yang

287   et al., 2018b) and are not discussed here. During 1850–1980, the long-range transport

288   contributions to the $PM_{2.5}$ burdens show increases and the contributions from ROW increased

289   the most among the tagged source regions over all four targeted receptor regions. Note that

290   aerosol emissions from North America contributed to the increase in European $PM_{2.5}$ burden

291   by 1.7 mg m^{-2} and sources from Europe were also responsible for the $PM_{2.5}$ burden increase by

292   1.0 mg m^{-2} in East Asia and 1.1 mg m^{-2} in South Asia. During 1980–2010, the long-range

293   transport from North America and Europe decreased, but that from East Asia and South Asia

294   increased. East Asia contributed 0.4–0.6 mg m^{-2} to the $PM_{2.5}$ burden increases in North

295   America, while Europe and South Asia contributed about 0.3 mg m^{-2}. In East Asia, 1.6 mg m^{-}

296   ^{2} of the $PM_{2.5}$ burden increase was attributed to South Asian sources and 0.8 mg m^{-2} of the

297    $PM_{2.5}$ burden increase in South Asia during this time period was due to increases in East Asian

298   emissions. From 2010 to 2017, owing to the clean air actions in China, contributions from East

299   Asia to the $PM_{2.5}$ burdens in the other three targeted regions decreased by 0.3–0.6 mg m^{-2}.

300   However, due to the continuous increases in South Asian emissions, South Asia still

301   contributed to the $PM_{2.5}$ burden increase in East Asia by 0.4 mg m^{-2} during this short time

302   period.

303   **3.3 Changes in effective radiative forcing due to aerosol-radiation interactions**

304   The variation in aerosols can have a significant impact on ERF through aerosol-radiation

305   and aerosol-cloud interactions. Figure 11 shows changes in ERF due to aerosol-radiation

306   interactions (ERF_{ari}) at the top of the atmosphere (TOA) that can be attributed to changes in

307   anthropogenic emissions from the tagged regions in the three key periods during 1850–2017.

308   Due to the increases in aerosols from 1850 to 1980, a large negative ERF_{ari} was located over

309   the major source regions and their downwind areas, with maximum ERF_{ari} changes being larger

310   than 2 W m^{-2} over eastern U.S., Europe and eastern China. In 2010, there were positive ERF_{ari}

311 changes (warming effect) by a maximum of 2 W m^{-2} in North America and Europe compared

312 to 1980, which were due to the decreases in anthropogenic aerosols in these two regions. The

313 positive ERF$_{ari}$ changes due to the decrease in North American aerosols extended across the

314 North Atlantic and caused an increase in incoming radiation by up to 0.5 W m^{-2} in Europe.

315 Similarly, the decrease in aerosols from Europe also led to a positive ERF$_{ari}$ change by up to

316 0.5 W m^{-2} in the downwind regions including Russia and northern China during 1980–2010.

317 Increases in aerosols in China during 1980–2010 and decreases during 2010–2017 produced

318 negative (cooling) and positive (warming) changes in ERF$_{ari}$, respectively, over eastern China

319 and North Pacific, which largely contradicted each other. The continuously growing aerosols

320 in South Asia induced negative ERF$_{ari}$ changes (cooling) in South Asia, Southeast Asia and

321 southern China during both 1980–2010 and 2010–2017. Note that in this study we only

322 quantify the ERF$_{ari}$ for the major emission regions based on the source tagging technique. The

323 quantification of ERF due to aerosol-cloud interactions (ERF$_{aci}$) requires additional simulations,

324 which could be further examined in future studies.

325 **4. Conclusions and Discussions**

326   Since the start of industrialization, aerosols have changed significantly in different regions

327 of the world driven by global economic development and air pollution control measures. It is

328 of great significance to quantify the contributions of aerosols from major emission source

329 regions and sectors during the key periods of substantial emission changes. In this study, the

330 Explicit Aerosol Source Tagging (EAST) technique is implemented in E3SMv1 to quantify the

331 variations in the concentrations, source contributions, and the subsequent effective radiative

332 forcing of anthropogenic aerosols in four major source regions (NAM, EUR, EAS and SAS)

333   during three key historical periods of emission changes (1850–1980, 1980–2010 and 2010–

334   2017).

335   Following the corresponding anthropogenic emission changes, $PM_{2.5}$ concentrations

336   reached its peak in 1980 in North America and Europe, while the peak of $PM_{2.5}$ in East Asia

337   occurred in 2010. The $PM_{2.5}$ from anthropogenic sources in South Asia continued growing

338   during 1850–2017. These changes in anthropogenic $PM_{2.5}$ were primarily dominated by

339   changes in sulfate aerosol. In North America and Europe, historical changes in anthropogenic

340    $PM_{2.5}$ were mainly caused by changes in emissions from local energy sector, followed by the

341   industrial sector, which increased from 1850 to 1980 and decreased afterward. In East Asia,

342   energy, industrial, and residential emissions contributed significantly to the increase in $PM_{2.5}$

343   from 1850 to 1980, then the local industrial sector caused the most increase from 1980 to 2010,

344   and declined from 2010 to 2017. For South Asia, the increase in $PM_{2.5}$ was mainly due to

345   emission changes in the residential sector from 1850 to 1980, then the increase in energy-

346   related emissions became dominant to the rise of $PM_{2.5}$ levels during 1980–2017.

347   Regional aerosol pollution comes from both local emissions and long-range transport of

348   remote emissions. Local emissions contribute the most in regions with high emissions, while

349   in regions with low emissions the long-distance transport plays an important role. Due to the

350   more efficient transport of air pollutants in the free troposphere, contributions of long-range

351   transport to column burden are greater than to the near-surface concentration over all four

352   targeted receptor regions. From 1850 to 1980, increases in emissions from North America

353   contributed to the increase in European $PM_{2.5}$ burden by 1.7 mg m^{-2} and emissions from Europe

354   were also responsible for the $PM_{2.5}$ burden increase by 1.0 mg m^{-2} in East Asia and 1.1 mg m^{-}

355 ^{2} in South Asia. From 1980 to 2010, the long-range transport from North America and Europe

356 decreased, while those from East Asia and South Asia increased. East Asia contributed 0.4–

357 0.6 mg m^{-2} to the PM$_{2.5}$ burden increases in North America, while Europe and South Asia

358 contributed about 0.3 mg m^{-2}. In East Asia, 1.6 mg m^{-2} of the PM$_{2.5}$ burden increase was

359 attributed to South Asian sources and 0.8 mg m^{-2} of the PM$_{2.5}$ burden increase in South Asia

360 during this time period was due to the increases in East Asian emissions. From 2010 to 2017,

361 the contributions from East Asia to the PM$_{2.5}$ burdens in the other three targeted regions

362 declined by 0.3–0.6 mg m^{-2} due to Clean Air actions in China. However, due to the continuous

363 increase of emissions in South Asia, the PM$_{2.5}$ burden in East Asia still increased by 0.4 mg m^{-}

364 ^{2}.

365   Changes in aerosols can have a significant impact on ERF, which further imposes an

366 impact on climate. Large negative ERF$_{ari}$ appeared over the major source regions and their

367 downwind areas during 1850–1980 due to the increases in aerosol emissions, with maximum

368 ERF$_{ari}$ changes being larger than 2 W m^{-2} over eastern North America, Europe and eastern

369 China. From 1980 to 2010, a positive ERF$_{ari}$ change caused by a decline in North American

370 aerosols extended over the North Atlantic, resulting in a warming of up to 0.5 W m^{-2} in Europe.

371 Meanwhile, a decline of aerosols in Europe also caused a warming of up to 0.5 W m^{-2} in Russia

372 and northern China. The changes in ERF$_{ari}$ from the increase (from 1980 to 2010) and decrease

373 (from 2010 to 2017) of aerosols in China had an opposite sign. The continuous aerosol

374 increases in South Asia from 1980 to 2017 resulted in negative ERF$_{ari}$ changes in South Asia,

375 Southeast Asia, and southern China.

376   This study provides an in-depth analysis of historical changes in anthropogenic aerosol

377 concentrations, compositions, source contributions and radiative impacts in the four major

378 emission source regions of the globe, which has important implications for the pollution

379 prevention/control measures and decision making for global collaboration. The spatial

380 distribution and changes in anthropogenic aerosols are similar to those reported in previous

381 studies (Hoesly, et al., 2018; Lim, et al., 2020). However, we also note that the E3SMv1 model

382 underestimates the near-surface $PM_{2.5}$ concentrations in Europe and East Asia, which could

383 lead to an underestimate of the corresponding radiative and climate impact. Our analysis

384 focuses on aerosols from anthropogenic emissions; however, with the increasing attention to

385 air quality in many countries around the world, anthropogenic aerosol concentrations are

386 declining and contributions from biomass burning aerosols are becoming more and more

387 important. The source contributions and impacts of biomass burning aerosols will be

388 investigated in our future work. Also, this study only quantifies the ERF_{ari} for individual major

389 emission regions based on the source tagging technique and radiation diagnostic calculations.

390 The quantification of ERF_{aci} requires additional simulations, which could be further examined

391 in future studies.

392   *Author contributions.* YY designed the research, added the tagging code and performed

393   simulations; SM analyzed the data. All authors including HW, PW, and HL discussed the

394   results and wrote the paper.

395

396   *Code and data availability.* The E3SMv1 model is available at https://github.com/E3SM-

397   Project/E3SM(last access:1 October 2022) (https://doi.org/10.11578/E3SM/dc.20180418.36;

398   E3SM Project, 2018). Our results can be made available upon request.

399

400   *Acknowledgments.* HW acknowledges the support by the U.S. Department of Energy (DOE),

401   Office of Science, Office of Biological and Environmental Research (BER), as part of the

402   Earth and Environmental System Modeling program. The Pacific Northwest National

403   Laboratory (PNNL) is operated for DOE by the Battelle Memorial Institute under contract

404   DE-AC05-76RLO1830.

405

406   *Financial support.* This study was supported by the National Key Research and

407   Development Program of China (grant 2020YFA0607803 and 2019YFA0606800), the

408   National Natural Science Foundation of China (grant 41975159), Jiangsu Science Fund for

409   Distinguished Young Scholars (grant BK20211541), and the Jiangsu Science Fund for

410   Carbon Neutrality (grant no. BK20220031).

411

412   *Conflict of interest.*

413   At least one of the (co-)authors is a member of the editorial board of ACP.

References

Abdul-Razzak, H. and Ghan, S. J.: A parameterization of aerosol activation, 2. Multiple
   aerosol types, J. Geophys. Res., 105, 6837– 6844,
   https://doi.org/10.1029/1999JD901161, 2000.

Akimoto, H.: Global Air Quality and Pollution, Science, 302, 1716–1719,
   https://doi.org/10.1126/science.1092666, 2003.

Anenberg, S. C., Horowitz, L. W., Tong, D. Q., and West, J. J.: An Estimate of the Global
   Burden of Anthropogenic Ozone and Fine Particulate Matter on Premature Human
   Mortality Using Atmospheric Modeling, Environ. Health Perspect., 118, 1189–1195,
   https://doi.org/10.1289/ehp.0901220, 2010.

Anenberg, S. C., West, J. J., Yu, H., Chin, M., Schulz, M., Bergmann, D., Bey, I., Bian, H.,
   Diehl, T., Fiore, A., Hess, P., Marmer, E., Montanaro, V., Park, R., Shindell, D.,
   Takemura, T., and Dentener, F.: Impacts of intercontinental transport of anthropogenic
   fine particulate matter on human mortality, Air. Qual. Atmos. Health., 7, 369–379,
   https://doi.org/10.1007/s11869-014-0248-9, 2014.

Carslaw, K. S., Gordon, H., Hamilton, D. S., Johnson, J. S., Regayre, L. A., Yoshioka, M.,
   and Pringle, K. J.: Aerosols in the Pre-industrial Atmosphere, Curr. Clim. Change Rep.,
   3, 1–15, https://doi.org/10.1007/s40641-017-0061-2, 2017.

Chen, D., Liao, H., Yang, Y., Chen, L., and Wang, H.: Simulated aging processes of black
   carbon and its impact during a severe winter haze event in the Beijing-Tianjin-Hebei
   region, Sci. Total Environ., 755, 142712,
   https://doi.org/10.1016/j.scitotenv.2020.142712, 2021.

Chin, M., Diehl, T., Ginoux, P., and Malm, W.: Intercontinental transport of pollution and
   dust aerosols: implications for regional air quality, Atmos. Chem. Phys., 7, 5501–5517,
   https://doi.org/10.5194/acp-7-5501-2007, 2007.

David, L. M., Ravishankara, A. R., Kodros, J. K., Pierce, J. R., Venkataraman, C., and
   Sadavarte, P.: Premature mortality due to $PM_{2.5}$ over India: Effect of atmospheric
   transport and anthropogenic emissions, Geohealth, 3, 2–10,
   https://doi.org/10.1029/2018GH000169, 2019.

Dey, S., Purohit, B., Balyan, P., Dixit, K., Bali, K., Kumar, A., Imam, F., Chowdhury, S.,
   Ganguly, D., Gargava, P., and Shukla, V. K.: A satellite-based high-resolution (1-km)
   ambient $PM_{2.5}$ database for India over two decades (2000–2019): applications for air
   quality management, Remote Sens., 12, 3872, https://doi.org/10.3390/rs12233872, 2022.

457 Finlayson-Pitts, B. J., and Pitts, J. N.: Tropospheric Air Pollution: Ozone, Airborne Toxics,
458   Polycyclic Aromatic Hydrocarbons, and Particles, Science, 276, 1045–1051,
459   https://doi.org/10.1126/science.276.5315.1045, 1997.
460
461 Gao, M., Beig, G., Song, S., Zhang, H., Hu, J., Ying, Q., Liang, F., Liu, Y., Wang, H., Lu, X.,
462   Zhu, T., Carmichael, G. R., Nielsen, C. P., McElroy, M. B.: The impact of power
463   generation emissions on ambient $PM_{2.5}$ pollution and human health in China and India,
464   Environ. Int., 121, 250-259, https://doi.org/10.1016/j.envint.2018.09.015, 2018.
465
466 Gao, J., Yang, Y., Wang, H., Wang, P., Li, H., Li, M., Ren, L., Yue, X., and Liao, H.: Fast
467   climate responses to emission reductions in aerosol and ozone precursors in China
468   during 2013–2017, Atmos. Chem. Phys., 22, 7131–7142, https://doi.org/10.5194/acp-
469   22-7131-2022, 2022.
470
471 Gao, J., Yang, Y., Wang, H., Wang, P., Li, B., Li, J., Wei, J., Gao, M., and Liao, H.: Climate
472   responses in China to domestic and foreign aerosol changes due to clean air actions
473   during 2013–2019, npj Clim. Atmos. Sci., 6, 160, https://doi.org/10.1038/s41612-023-
474   00488-y, 2023.
475
476 Gelaro, R., McCarty, W., Suárez, M. J., Todling, R., Molod, A., Takacs, L., Randles, C. A.,
477   Darmenov, A., Bosilovich, M. G., Reichle, R., Wargan, K., Coy, L., Cullather, R.,
478   Draper, C., Akella, S., Buchard, V., Conaty, A., da Silva, A. M., Gu, W., Kim, G.,
479   Koster, R., Lucchesi, R., Merkova, D., Nielsen, J. E., Partyka, G., Pawson, S., Putman,
480   W., Rienecker, M., Schubert, S. D., Sienkiewicz, M., and Zhao, B.: The Modern-Era
481   Retrospective Analysis for Research and Applications, Version 2 (MERRA-2), J.
482   Climate, 30, 5419–5454, https://doi.org/10.1175/JCLI-D-16-0758.1, 2017.
483
484 Ghan, S. J.: Technical Note: Estimating aerosol effects on cloud radiative forcing, Atmos.
485   Chem. Phys., 13, 9971–9974, https://doi.org/10.5194/acp-13-9971-2013, 2013.
486
487 Ghan, S. J. and Zaveri, R. A.: Parameterization of optical properties for hydrated internally
488   mixed aerosol, J. Geophys. Res.-Atmos., 112, D10201,
489   https://doi.org/10.1029/2006JD007927, 2007.
490
491 Golaz, J. C., Caldwell, P. M., Van Roekel, L. P., Petersen, M. R., Tang, Q., Wolfe, J. D.,
492   Abeshu, G., Anantharaj, V., Asay-Davis, X. S., Bader, D. C., Baldwin, S. A., Bisht, G.,
493   Bogenschutz, P. A., Branstetter, M., Brunke, M. A., Brus, S. R., Burrows, S. M.,
494   Cameron-Smith, P. J., Donahue, A. S., Deakin, M., Easter, R. C., Evans, K. J., Feng, Y.,
495   Flanner, M., Foucar, J. G., Fyke, J. G., Griffin, B. M., Hannay, C., Harrop, B. E.,
496   Hoffman, M. J., Hunke, E. C., Jacob, R. L., Jacobsen, D. W., Jeffery, N., Jones, P. W.,
497   Keen, N. D., Klein, S. A., Larson, V. E., Leung, L. R., Li, H. Y., Lin, W., Lipscomb, W.
498   H., Ma, P., Mahajan, S., Maltrud, M. E., Mametjanov, A., McClean, J. L., McCoy, R.
499   B., Neale, R. B., Price, S. F., Qian, Y., Rasch, P. J., Eyre, J. E. J. R., Riley, W. J.,
500   Ringler, T. D., Roberts, A. F., Roesler, E. L., Salinger, A. G., Shaheen, Z., Shi, X.,

Singh, B., Tang, J., Taylor, M. A., Thornton, P. E., Turner, A. K., Veneziani, M., Wan, H., Wang, H., Wang, S., Williams, D. N., Wolfram, P. J., Worley, P. H., Xie, S., Yang Y., Yoon, J., Zelinka, M. D., Zender, C. S., Zeng, X., Zhang, C., Zhang, K., Zhang, Y., Zheng, X., Zhou, T., and Zhu, Q.: The DOE E3SM Coupled Model Version 1: Overview and Evaluation at Standard Resolution, J. Adv. Model. Earth Syst., 11, 2089–2129. https://doi.org/10.1029/2018MS001603, 2019.

Guttikunda, S., and Nishadh, K. A.: Evolution of India's $PM_{2.5}$ pollution between 1998 and 2020 using global reanalysis fields coupled with satellite observations and fuel consumption patterns, Environ. Sci. Atmos., 2, 1502-1515, https://doi.org/10.1039/D2EA00027J, 2022.

Hoesly, R. M., Smith, S. J., Feng, L., Klimont, Z., Janssens-Maenhout, G., Pitkanen, T., Seibert, J. J., Vu, L., Andres, R. J., Bolt, R. M., Bond, T. C., Dawidowski, L., Kholod, N., Kurokawa, J., Li, M., Liu, L., Lu, Z., Moura, M. C. P., O'Rourke, P. R., and Zhang, Q.: Historical (1750–2014) anthropogenic emissions of reactive gases and aerosols from the Community Emissions Data System (CEDS), Geosci. Model Dev., 11, 369–408, https://doi.org/10.5194/gmd-11-369-2018, 2018.

Jaffe, D., Anderson, T., Covert, D., Kotchenruther, R., Trost, B., Danielson, J., Simpson, W., Berntsen, T., Karlsdottir, S., Blake, D., Harris, J., Carmichael, G., and Uno, I.: Transport of Asian air pollution to North America, Geophys. Res. Lett., 26, 711–714, https://doi.org/10.1029/1999GL900100, 1999.

Li, C., McLinden, C., Fioletov, V., Krotkov, N., Carn, S., Joiner, J., Streets, D., He, H., Ren, X., Li, Z., and Dickerson, R.: India Is Overtaking China as the World's Largest Emitter of Anthropogenic Sulfur Dioxide, Sci. Rep., 7, 14304, https://doi.org/10.1038/s41598-017-14639-8, 2017.

Li, H., Yang, Y., Wang, H., Li, B., Wang, P., Li, J., and Liao, H.: Constructing a spatiotemporally coherent long-term $PM_{2.5}$ concentration dataset over China using a machine learning approach, Sci. Total Environ., 765, 144263, https://doi.org/10.1016/j.scitotenv.2020.144263, 2021.

Liao, H., Chang, W., and Yang, Y.: Climatic effects of air pollutants over China: A review, Adv. Atmos. Sci., 32, 115–139, https://doi.org/10.1007/s00376-014-0013-x, 2015.

Lim, C.-H., Ryu, J., Choi, Y., Jeon, S. W., and Lee, W.-K.: Understanding global PM2.5 concentrations and their drivers in recent decades (1998–2016), Environ. Int., 144, 106011, https://doi.org/10.1016/j.envint.2020.106011, 2020.

Lin, J., Pan, D., Davis, S. J., Zhang, Q., He, K., Wang, C., Streets, D. G., Wuebbles, D. J., and Guan, D.: China's international trade and air pollution in the United States, Proc. Natl. Acad. Sci., 111, 1736–1741, https://doi.org/10.1073/pnas.1312860111, 2014.

545

546 Liu, J., and Mauzerall, D.: Estimating the average time for inter-continental transport of air
547   pollutants, Geophys. Res. Lett., 32, L11814, https://doi.org/10.1029/2005GL022619,
548   2005.

549

550 Liu, J., Mauzerall, D. L., Horowitz, L. W., Ginoux, P., and Fiore, A. M.: Evaluating inter-
551   continental transport of fine aerosols: (1) Methodology, global aerosol distribution and
552   optical depth, Atmos. Environ., 43, 4327–4338,
553   https://doi.org/10.1016/j.atmosenv.2009.03.054, 2009.

554

555 Lohmann, U., and Feichter, J.: Global indirect aerosol effects: a review, Atmos. Chem. Phys.,
556   5, 715–737, https://doi.org/10.5194/acp-5-715-2005, 2005.

557

558 Lou, S., Yang, Y., Wang, H., Smith, S. J., Qian, Y., and Rasch, P. J.: Black carbon amplifies
559   haze over the North China Plain by weakening the East Asian winter monsoon,
560   Geophys. Res. Lett., 46, 452–460, https://doi.org/10.1029/2018GL080941, 2019.

561

562 Navinya, C. D., Vinoj, V. and Pandey, S. K.: Evaluation of $PM_{2.5}$ Surface Concentrations
563   Simulated by NASA's MERRA Version 2 Aerosol Reanalysis over India and its relation
564   to the Air Quality Index, Aerosol Air Qual. Res., 20, 1329–1339,
565   https://doi.org/10.4209/aaqr.2019.12.0615, 2020.

566

567 Pöschl, U.: Atmospheric Aerosols: Composition, Transformation, Climate and Health
568   Effects, Angew. Chem. Int. Ed., 44, 7520–7540,
569   https://doi.org/10.1002/anie.200501122, 2005.

570

571 Rasch, P. J., Xie, S., Ma, P.-L., Lin, W., Wang, H., Tang, Q., Burrows, S. M., Caldwell, P.,
572   Zhang, K., Easter, R. C., Cameron-Smith, P., Singh, B., Wan, H., Golaz, J.-C., Harrop,
573   B. E., Roesler, E., Bacmeister, J., Larson, V. E., Evans, K. J., Qian, Y., Taylor, M.,
574   Leung, L. R., Zhang, Y., Brent, L., Branstetter, M., Hannay, C., Mahajan, S.,
575   Mametjanov, A., Neale, R., Richter, J. H., Yoon, J.-H., Zender, C. S., Bader, D.,
576   Flanner, M., Foucar, J. G., Jacob, R., Keen, N., Klein, S. A., Liu, X., Salinger, A. G.,
577   Shrivastava, M., and Yang, Y.: An overview of the atmospheric component of the
578   Energy Exascale Earth System Model, J. Adv. Model. Earth Sy., 11, 2377–2411,
579   https://doi.org/10.1029/2019MS001629, 2019.

580

581 Ren, L., Yang, Y., Wang, H., Wang, P., Chen, L., Zhu, J., and Liao, H.: Aerosol transport
582   pathways and source attribution in China during the COVID-19 outbreak, Atmos. Chem.
583   Phys., 21, 15431–15445, https://doi.org/10.5194/acp-21-15431-2021, 2021.

584

585 Rosenfeld, D., Lohmann, U., Raga, G. B., Kulmala, M., Fuzzi, S., Reissell, A., and Andreae,
586   M. O.: Flood or Drought: How Do Aerosols Affect Precipitation?, Science, 321, 1309–
587   1313, https://doi.org/10.1126/science.1160606, 2008.

588

589 Singh, T., Matsumi, Y., Nakayama, T., Hayashida, S., Patra, P. K., Yasutomi, N., Kajino, M.,
590   Yamaji, K., Khatri, P., Takigawa, M., Araki, H., Kurogi, Y., Kuji, M., Muramatsu, K.,
591   Imasu, R., Ananda, A., Arbain, A. A., Ravindra, K., Bhardwaj, S., Kumar, S., Mor, S.,
592   Dhaka, S. K., Dimri, A. P., Sharma, A., Singh, N., Bhatti, M. S., Yadav, R., Vatta, K.,
593   and Mor, S.: Very high particulate pollution over northwest India captured by a high-
594   density in situ sensor network, Sci. Rep., 13, 13201, https://doi.org/10.1038/s41598-023-
595   39471-1, 2023.

597 Smith, S. J., van Aardenne, J., Klimont, Z., Andres, R. J., Volke, A., and Arias, S. D.:
598   Anthropogenic sulfur dioxide emissions: 1850–2005, Atmos. Chem. Phys., 11, 1101–
599   1116, https://doi.org/10.5194/acp-11-1101-2011, 2011.

601 Stohl, A., and Trickl, T.: A textbook example of long-range transport: Simultaneous
602   observation of ozone maxima of stratospheric and North American origin in the free
603   troposphere over Europe, J. Geophys. Res., 104, 30445–30462,
604   https://doi.org/10.1029/1999JD900803, 1999.

606 van Marle, M. J. E., Kloster, S., Magi, B. I., Marlon, J. R., Daniau, A.-L., Field, R. D.,
607   Arneth, A., Forrest, M., Hantson, S., Kehrwald, N. M., Knorr, W., Lasslop, G., Li, F.,
608   Mangeon, S., Yue, C., Kaiser, J. W., and van der Werf, G. R.: Historic global biomass
609   burning emissions for CMIP6 (BB4CMIP) based on merging satellite observations with
610   proxies and fire models (1750–2015), Geosci. Model Dev., 10, 3329–3357,
611   https://doi.org/10.5194/gmd-10-3329-2017, 2017.

613 Wang, H., Rasch, P. J., Easter, R. C., Singh, B., Zhang, R., Ma, P.-L., Qian, Y., Ghan, S. J.,
614   and Beagley, N.: Using an explicit emission tagging method in global modeling of
615   source-receptor relationships for black carbon in the Arctic: Variations, sources, and
616   transport pathways, J. Geophys. Res. Atmos., 119, 12888–12909,
617   https://doi.org/10.1002/2014JD022297, 2014.

619 Wang, H., Easter, R. C., Zhang, R., Ma, P.-L., Singh, B., Zhang, K., Ganguly, D., Rasch, P .
620   J., Burrows, S. M., Ghan, S. J., Lou, S., Qian, Y ., Yang, Y ., Feng, Y ., Flanner, M.,
621   Leung, L. R., Liu, X., Shrivastava, M., Sun, J., Tang, Q., Xie, S., and Yoon, J.-H.:
622   Aerosols in the E3SM Version 1: New developments and their impacts on radiative
623   forcing, J. Adv. Model. Earth Syst., 12, e2019MS001851,
624   https://doi.org/10.1029/2019MS001851, 2020.

626 Wang, P., Yang, Y., Xue, D., Ren, L., Tang, J., Leung, L. R., and Liao, H.: Aerosols overtake
627   greenhouse gases causing a warmer climate and more weather extremes toward carbon
628   neutrality, Nat. Commun., 14, 7257, https://doi.org/10.1038/s41467-023-42891-2, 2023.

630 Wang, Y., Liu, X., Hoose, C., and Wang, B.: Different contact angle distributions for
631   heterogeneous ice nucleation in the Community Atmospheric Model version 5, Atmos.
632   Chem. Phys., 14, 10411–10430, https://doi.org/10.5194/acp-14-10411-2014, 2014.

Yang, Y., Wang, H., Smith, S. J., Easter, R., Ma, P.-L., Qian, Y., Yu, H., Li, C., and Rasch, P. J.: Global source attribution of sulfate concentration and direct and indirect radiative forcing, Atmos. Chem. Phys., 17, 8903–8922, https://doi.org/10.5194/acp-17-8903-2017, 2017.

Yang, Y., Wang, H., Smith, S. J., Zhang, R., Lou, S., Qian, Y., Ma, P., and Rasch P. J.: Recent intensification of winter haze in China linked to foreign emissions and meteorology, Sci. Rep., 8, 2107, https://doi.org/10.1038/s41598-018-20437-7, 2018a.

Yang, Y., Wang, H., Smith, S. J., Zhang, R., Lou, S., Yu, H., Li, C., and Rasch, P. J.: Source Apportionments of Aerosols and Their Direct Radiative Forcing and Long-Term Trends Over Continental United States, Earth's Future, 6, 793–808, https://doi.org/10.1029/2018EF000859, 2018b.

Yang, Y., Ren, L., Li, H., Wang, H., Wang, P., Chen, L., Yue, X., and Hong, L.: Fast climate responses to aerosol emission reductions during the COVID-19 pandemic, Geophys. Res. Lett., 47, e2020GL089788, https://doi.org/10.1029/2020GL089788, 2020a.

Yang, Y., Lou, S., Wang, H., Wang, P., and Liao, H.: Trends and source apportionment of aerosols in Europe during 1980–2018, Atmos. Chem. Phys., 20, 2579–2590, https://doi.org/10.5194/acp-20-2579-2020, 2020b.

Yang, Y., Ren, L., Wu, M., Wang, H., Song, F., Leung, L. R., Hao, X., Li, J., Chen, L., Li, H., Zeng, L., Zhou, Y., Wang, P., Liao, H., Wang, J., and Zhou, Z.-Q.: Abrupt emissions reductions during COVID-19 contributed to record summer rainfall in China, Nat. Commun., 13, 959, https://doi.org/10.1038/s41467-022-28537-9, 2022a

Yang, Y., Zeng, L., Wang, H., Wang, P., and Liao, H.: Dust pollution in China affected by different spatial and temporal types of El Niño, Atmos. Chem. Phys., 22, 14489–14502, https://doi.org/10.5194/acp-22-14489-2022, 2022b.

Yang, Y., Zeng, L., Wang, H., Wang, P., and Liao, H.: Climate effects of future aerosol reductions for achieving carbon neutrality in China, Sci. Bull., 68, 902–905, https://doi.org/10.1016/j.scib.2023.03.048, 2023..

Zeng, L., Yang, Y., Wang, H., Wang, J., Li, J., Ren, L., Li, H., Zhou, Y., Wang, P., and Liao, H.: Intensified modulation of winter aerosol pollution in China by El Niño with short duration, Atmos. Chem. Phys., 21, 10745–10761, https://doi.org/10.5194/acp-21-10745-2021, 2021.

Zhang, Q., Jiang, X., Tong, D., Davis, S. J., Zhao, H., Geng, G., Feng, T., Zheng, B., Lu, Z., Streets, D. G., Ni, R., Brauer, M., van Donkelaar, A., Martin, R. V., Huo, H., Liu, Z., Pan, D., Kan, H., Yan, Y., Lin, J., He, K., and Guan, D.: Transboundary health impacts

677  of transported global air pollution and international trade, Nature, 543, 705–709,

678  https://doi.org/10.1038/nature21712, 2017.

679

680 Zheng, B., Tong, D., Li, M., Liu, F., Hong, C., Geng, G., Li, H., Li, X., Peng, L., Qi, J., Yan,

681  L., Zhang, Y., Zhao, H., Zheng, Y., He, K., and Zhang, Q.: Trends in China's

682  anthropogenic emissions since 2010 as the consequence of clean air actions, Atmos.

683  Chem. Phys., 18, 14095–14111, https://doi.org/10.5194/acp-18-14095- 2018, 2018.

684
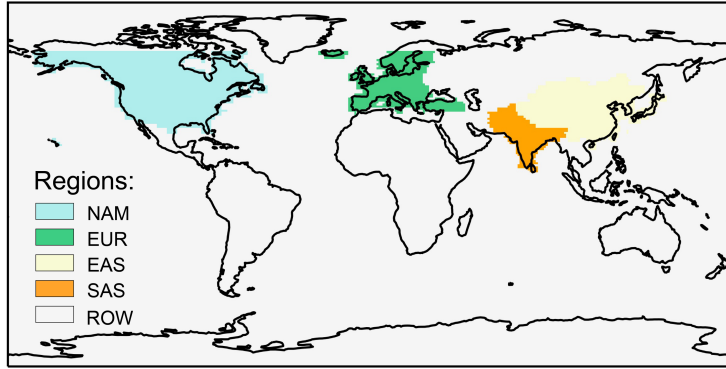
685

686 **Figure 1.** Tagged source regions (NAM: North America; EUR: Europe; EAS: East Asia; SAS:
687 South Asia; ROW: rest of the world).

688
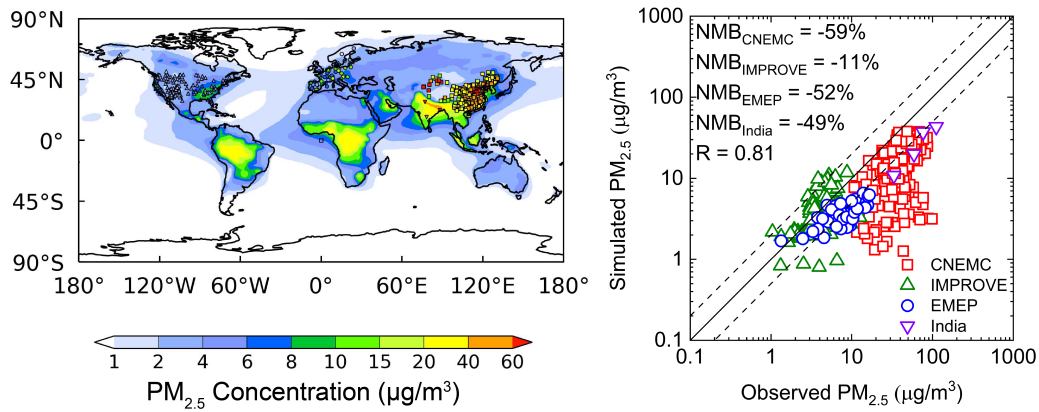
Figure 2. Spatial distribution (left panel) and scatter plot (right) between the simulated and observed annual mean near-surface PM$_{2.5}$ concentrations (µg/m³) in 2017. Observational data are from IMPROVE (triangle), EMEP (circle), India (inverted triangle) and CNEMC (square). The solid line marks the 1:1 ratio and dashed lines mark the 1:2 and 2:1 ratios. Normalized mean bias (NMB) and correlation coefficient (R) between observation and simulation are shown on the right panel. $NMB = 100\% \times \sum(M_i - O_i)/\sum O_i$, where M_i and O_i are the modeled and observed values at site i , respectively.

696
697

698
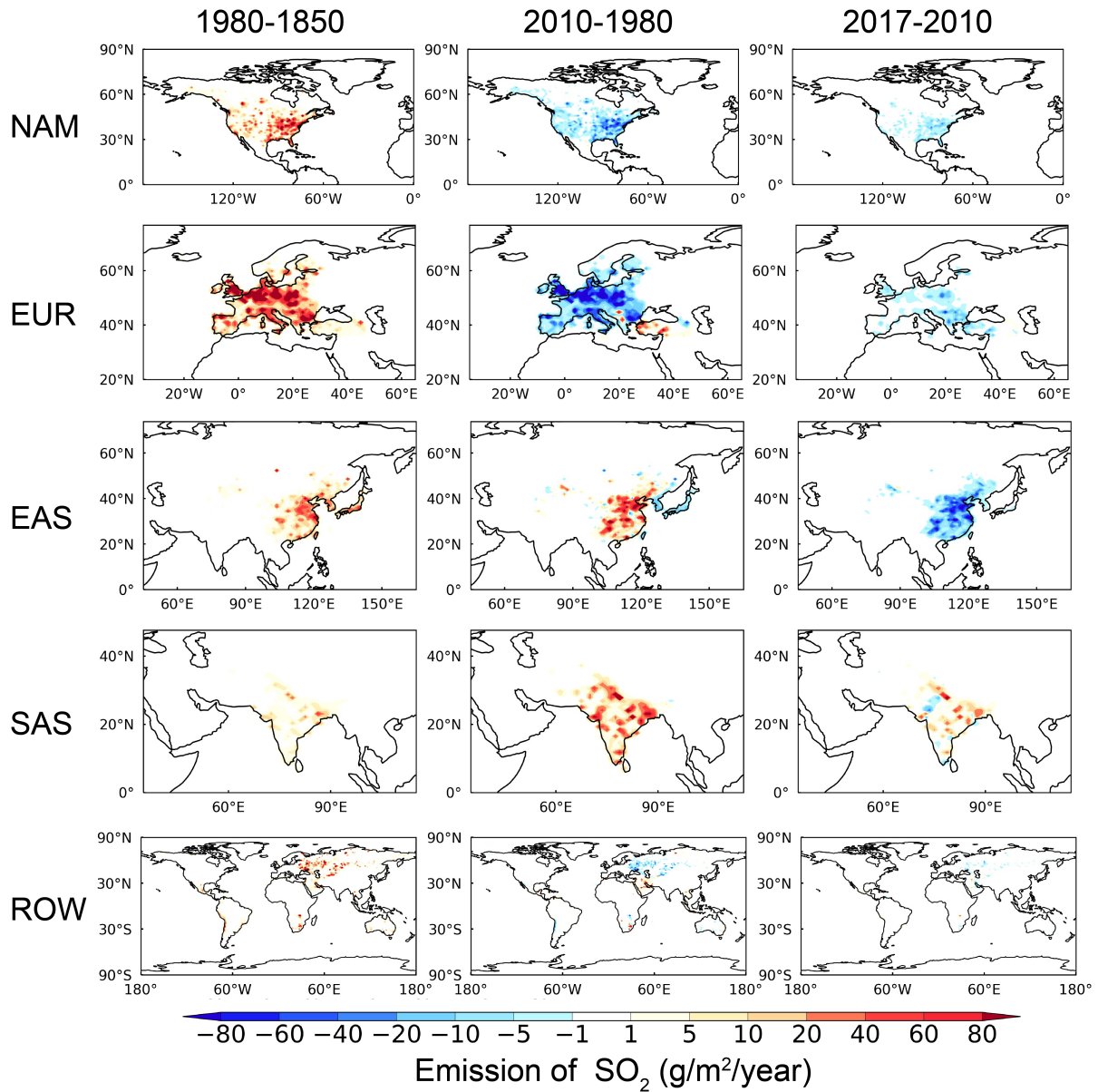
Figure 3. Changes in anthropogenic sulfur dioxide (SO₂) emissions (g/m²/year) between 1850
and 1980 (left), between 1980 and 2010 (middle), and between 2010 and 2017 (right) in the 5
tagged source regions (NAM, EUR, EAS, SAS and ROW from top to bottom).

702
703
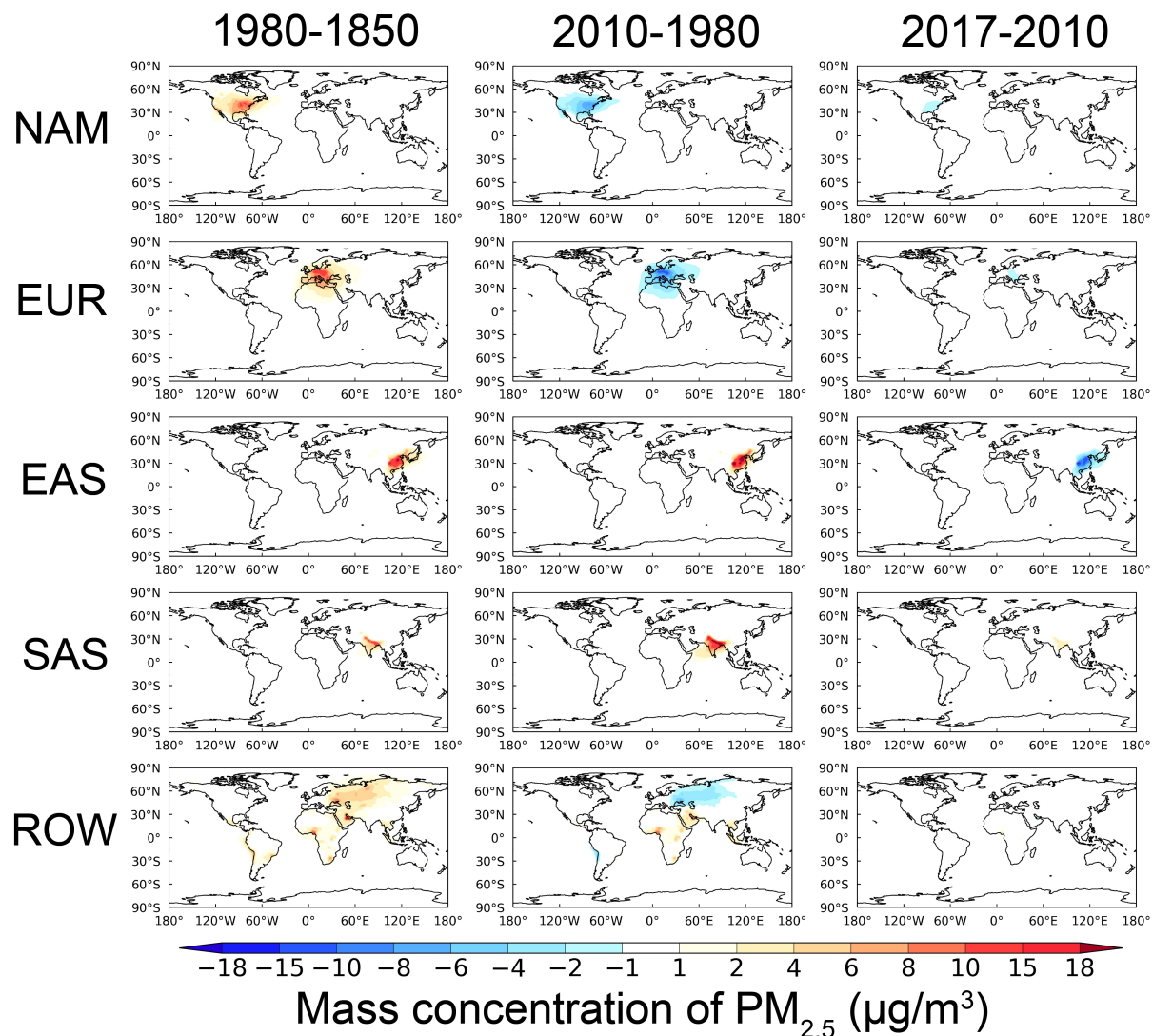
Figure 4. Changes in near-surface mass concentration (μg/m³) of anthropogenic PM₂.₅ contributed by the 5 tagged source regions (NAM, EUR, EAS, SAS and ROW from top to bottom) between 1850 and 1980 (left), between 1980 and 2010 (middle), and between 2010 and 2017 (right).
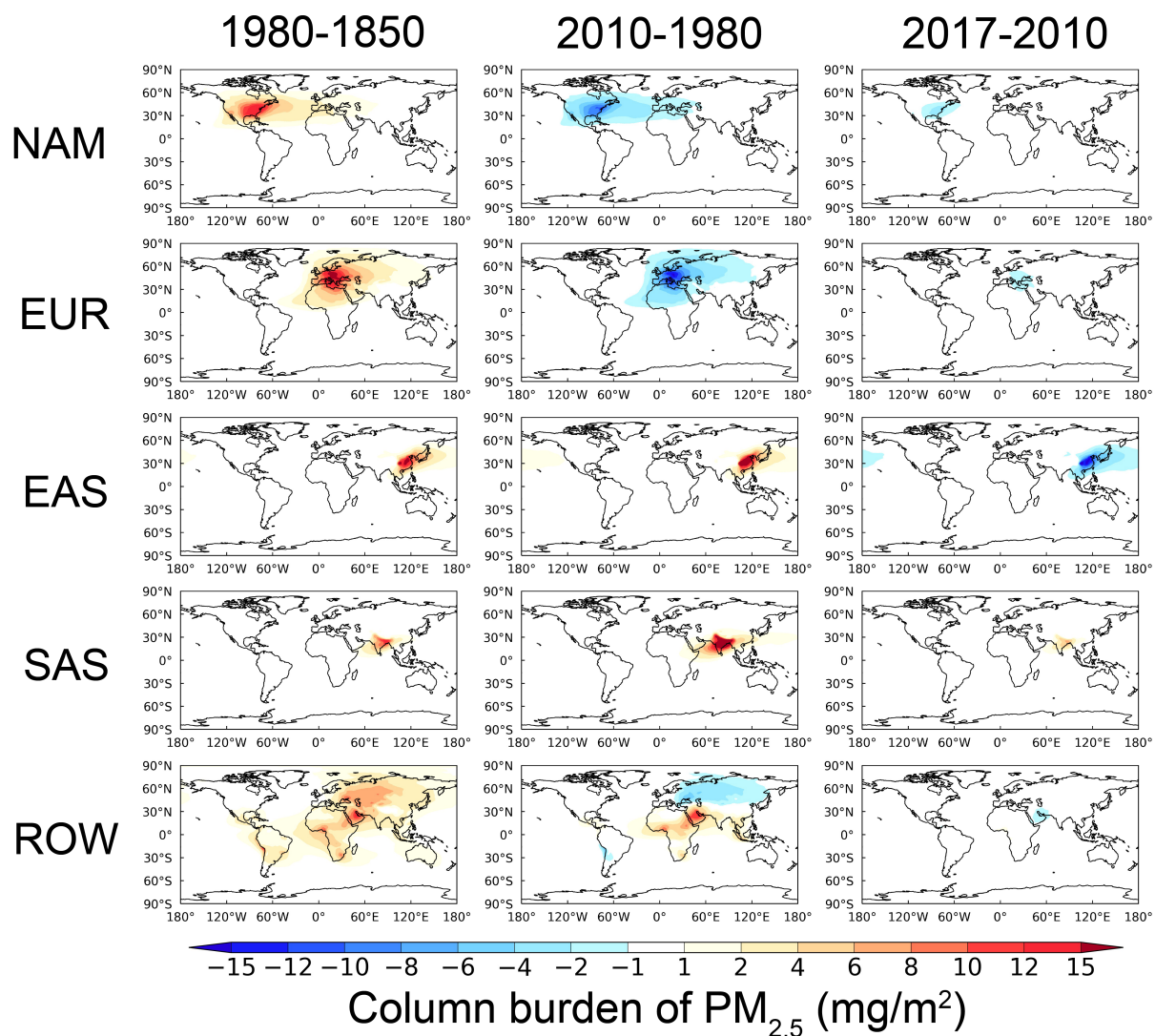
Figure 5. Changes in column burden (mg/m^2) of anthropogenic PM$_{2.5}$ contributed by the 5 tagged source regions (NAM, EUR, EAS, SAS and ROW from top to bottom) between 1850 and 1980 (left), between 1980 and 2010 (middle), and between 2010 and 2017 (right).

710

711

712

713

714
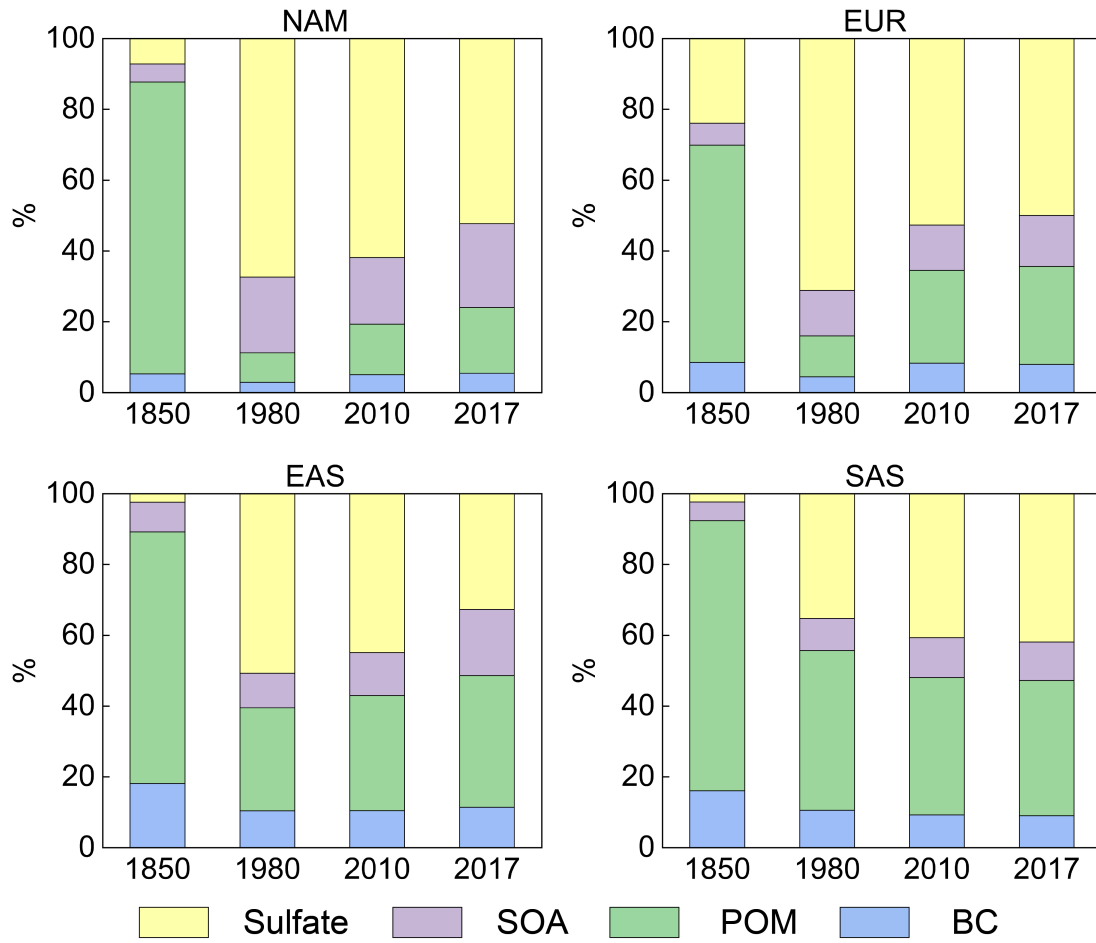
Figure 6. Percentage contributions (%) of aerosol species including BC, POM, SOA and sulfate to the near-surface mass concentrations of $PM_{2.5}$ averaged over the four major emission source regions (NAM, EUR, EAS and SAS) in the focused four years (1850, 1980, 2010 and 2017).

721
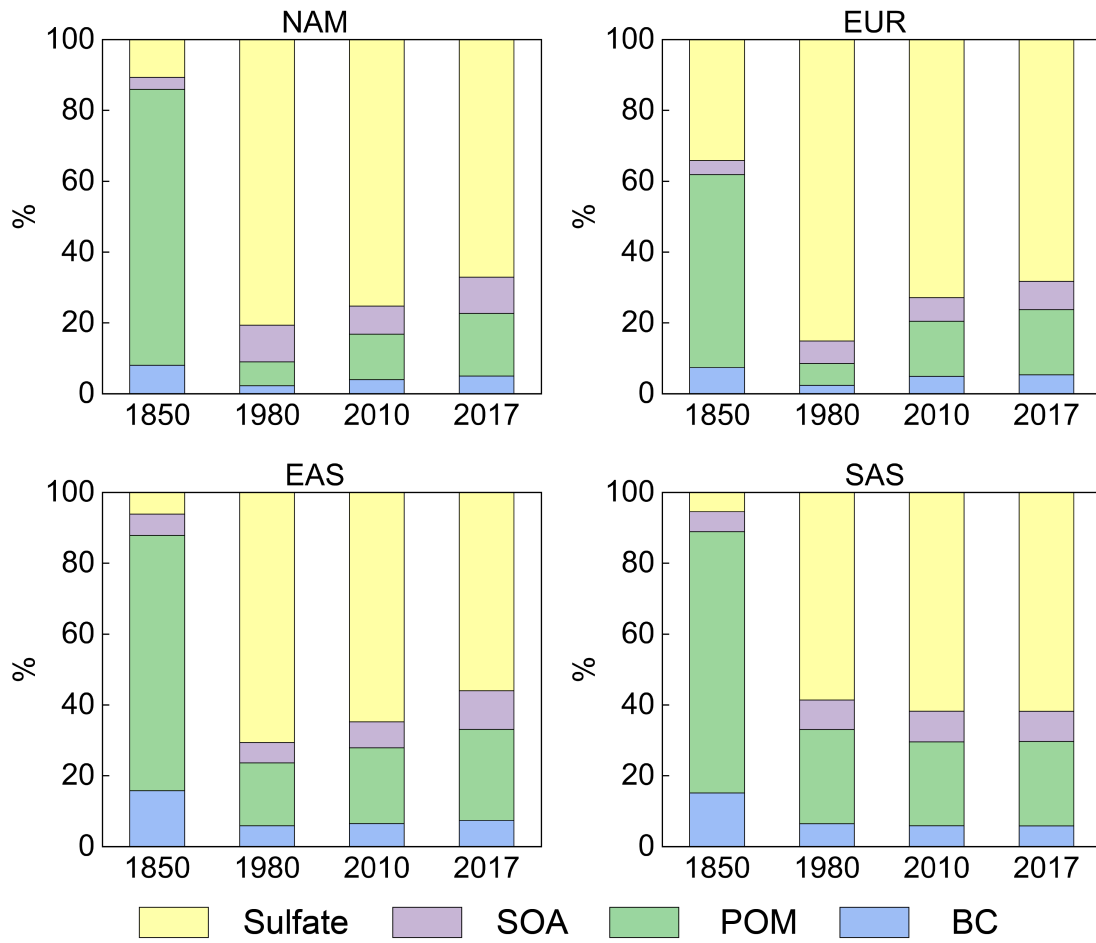
Figure 7. Percentage contributions (%) of aerosol species including BC, POM, SOA and
sulfate to the column burden of PM$_{2.5}$ averaged over the four major emission source regions
(NAM, EUR, EAS and SAS) in the focused four years (1850, 1980, 2010 and 2017).

725
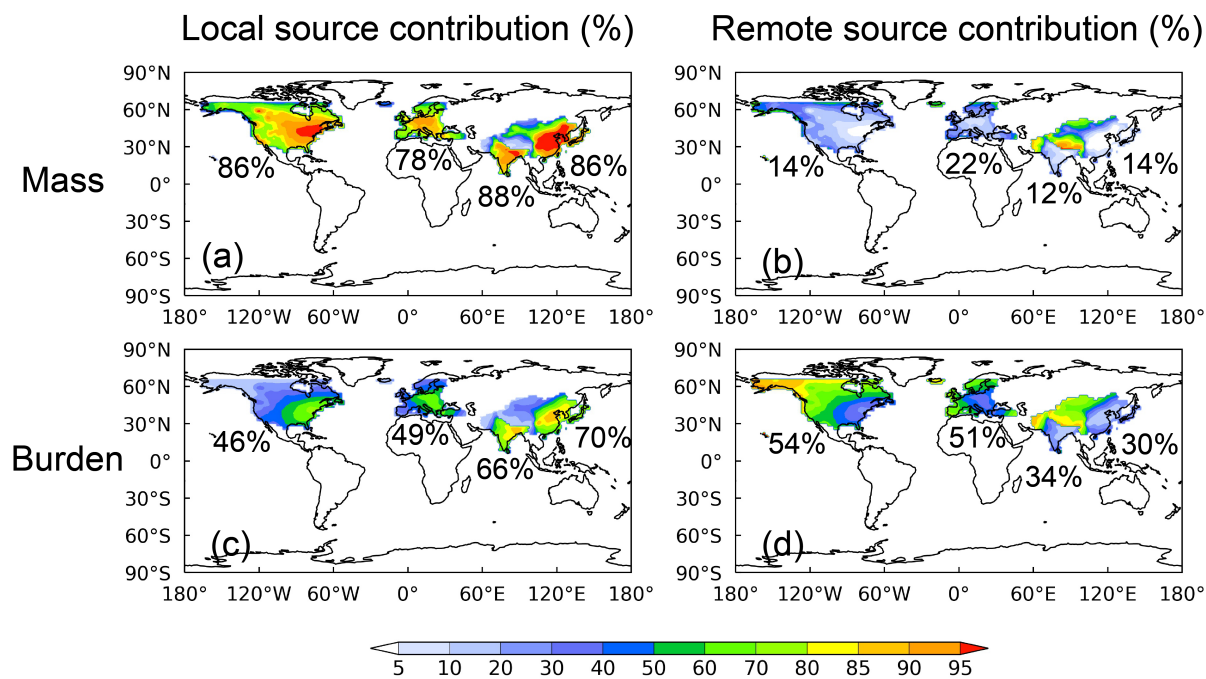
Figure 8. Relative contributions (%) from (a, c) local and (b, d) remote anthropogenic emissions to the near-surface mass concentrations and column burdens of $PM_{2.5}$ in the four targeted regions (NAM, EUR, EAS and SAS) in 2010. Numbers marked on the figure are the regional average over the four individual targeted regions.
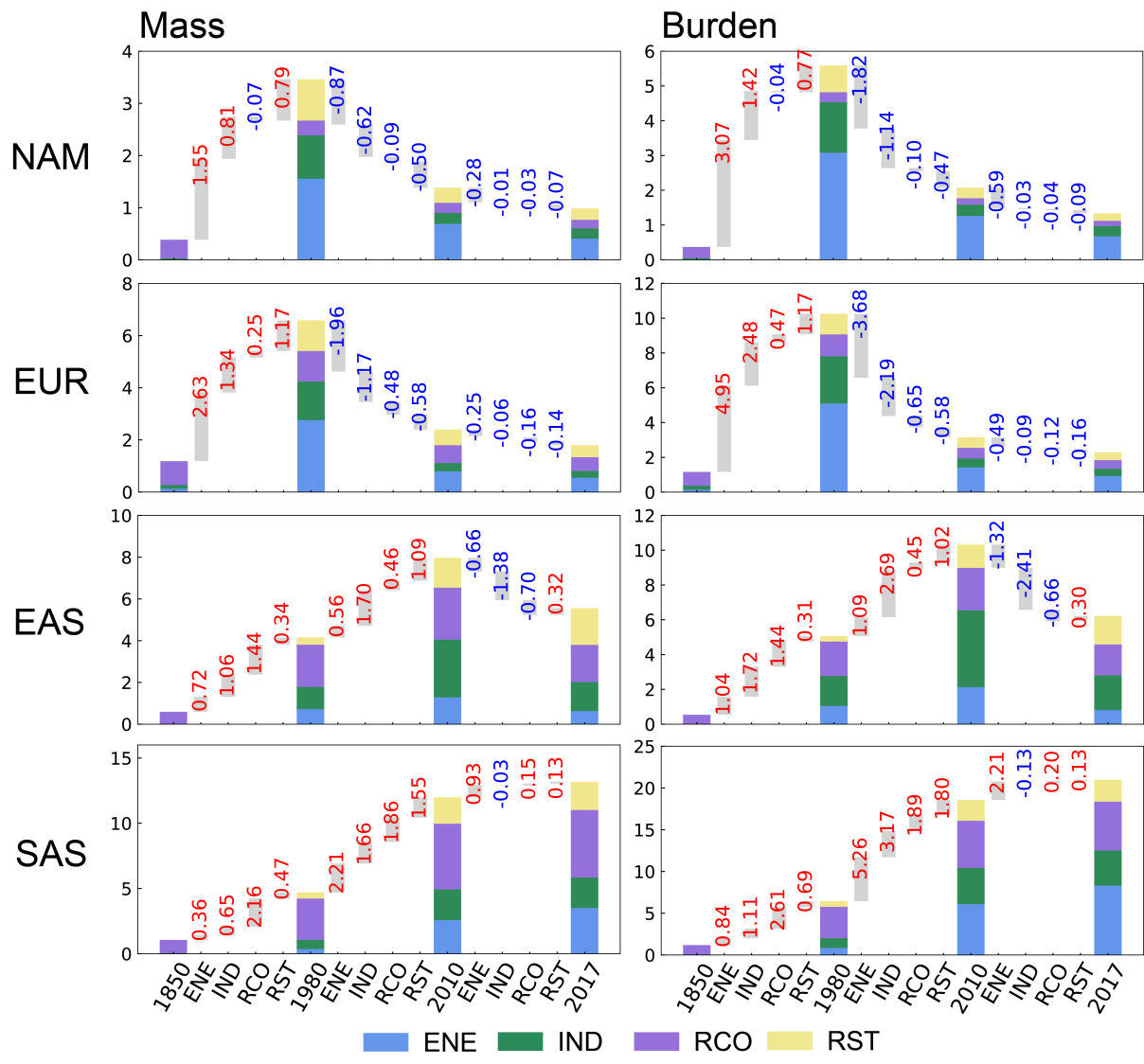
Figure 9. Local source contributions from four individual emission sectors (ENE, IND, RCO and RST) to the near-surface mass concentrations (μg/m³, left) and column burdens (mg/m², right) of anthropogenic PM$_{2.5}$ in the four targeted regions (NAM, EUR, EAS and SAS from top to bottom) for years 1850, 1980, 2010 and 2017 (in color bars). Grey bar and numbers in between two years show the change in sector contributions. Positive values are shown in red and negative values are shown in blue.
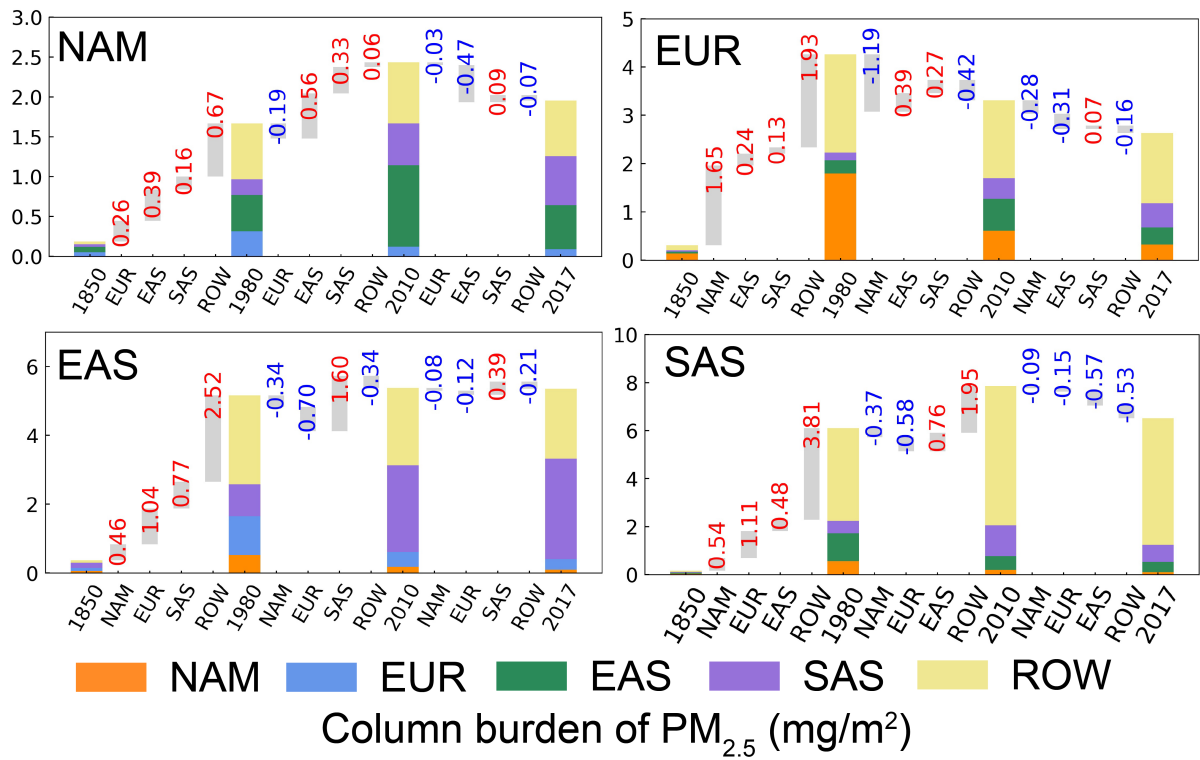
Figure 10. Same as Figure 9, but for contributions from the remote tagged source regions to the column burdens (mg/m²) of anthropogenic PM$_{2.5}$ in the four targeted regions (NAM, EUR, EAS and SAS).
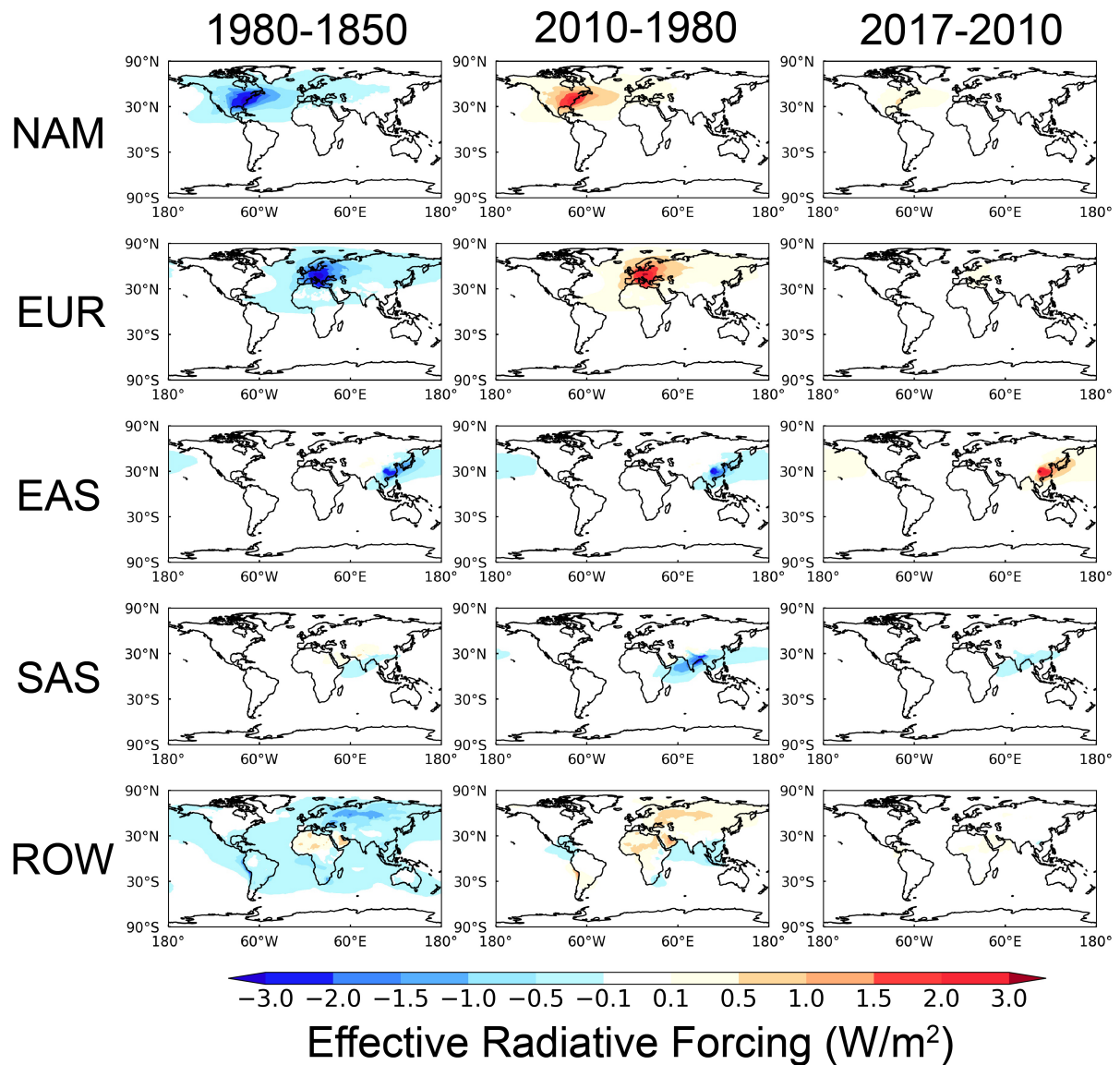
Figure 11. Changes in effective radiative forcing (W m^{-2}) at the top of the atmosphere due to aerosol-radiation interactions between 1850 and 1980 (left), between 1980 and 2010 (middle), and between 2010 and 2017 (right) attributed to the changes in anthropogenic emissions from NAM, EUR, EAS, SAS and ROW (from top to bottom).